

Direct observation of attractive skyrmions and skyrmion clusters in a cubic helimagnet Cu_2OSeO_3

J. C. Loudon,^{1,*} A. O. Leonov,^{2,3,4,†} A. N. Bogdanov,^{3,4} M. Ciomaga Hatnean,⁵ and G. Balakrishnan⁵

¹*Department of Materials Science and Metallurgy,
27 Charles Babbage Road, Cambridge, CB3 0FS, United Kingdom*

²*Department of Chemistry, Faculty of Science, Hiroshima University
Kagamiyama, Higashi Hiroshima, Hiroshima 739-8526, Japan*

³*Center for Chiral Science, Hiroshima University 1-3-1 Kagamiyama, Higashi Hiroshima, Hiroshima 739-8526, Japan*

⁴*IFW Dresden, Postfach 270016, D-01171 Dresden, Germany*

⁵*Department of Physics, University of Warwick, Coventry CV4 7AL, United Kingdom*

(Dated: June 29, 2022)

We report the discovery of *attractive* magnetic skyrmions and their clusters in non-centrosymmetric ferromagnets. These specific three-dimensional solitons have been predicted to exist in the cone phases of chiral ferromagnets (J.Phys:Condens. Matter **28** (2016) 35LT01) and are fundamentally different from the common axisymmetric repulsive skyrmions arising in the magnetically saturated states. We present real-space images of these skyrmion clusters in thin (~ 70 nm) single-crystal samples of Cu_2OSeO_3 taken using transmission electron microscopy and develop a phenomenological theory describing this type of skyrmion.

1. In magnetic compounds lacking inversion symmetry, the handedness of the underlying crystal structure induces a specific asymmetric exchange coupling (a *Dzyaloshinskii-Moriya* (DM) interaction¹) stabilizing long-period spatial modulations of the magnetization with a fixed rotation sense^{1,2}. In the last few years, a renewed interest in chiral helimagnetism has been inspired by the discovery of two-dimensional localized modulations (commonly called *chiral skyrmions*)^{3-5,7}. In the most nonlinear physical systems, similar two-dimensional localized states are radially unstable and collapse spontaneously into linear singularities. Chiral interactions provide a unique stabilization mechanism, protecting two-dimensional localized states from radial instability^{4,7}. That is why noncentrosymmetric magnets and other chiral condensed matter systems are of special interest in fundamental physics and mathematics as a particular class of materials where skyrmions can exist^{8,9}.

The chiral skyrmions that were theoretically introduced in^{3,4} and experimentally investigated in nanolayers of chiral ferromagnets^{5,7} are axisymmetric nanoscaled solitons embedded in the saturated phase. Recently, fundamentally different solitonic states have been investigated mathematically in transversely modulated phases (*cone* phases) of chiral ferromagnets¹². Contrary to common axisymmetric skyrmions, these three-dimensional chiral solitons are inhomogeneous along their axes and asymmetric in the basic planes (Fig. 1 a-c)¹². They are mutually attractive and tend to produce multi-skyrmion bound states (*clusters*)^{12,13}. In the phase diagrams of cubic helimagnets and uniaxial ferromagnets with D_n and C_n symmetries, the saturated states are contiguous with extended areas of the cone phase, helical modulations with the propagation direction along the applied magnetic field (Fig.1 (d))^{7,11}. Axisymmetric skyrmions inhabiting the saturated states continuously transform into the non-axisymmetric solitons during the second-order transition at critical field H_C (Fig.1 (d)). Theoretically,

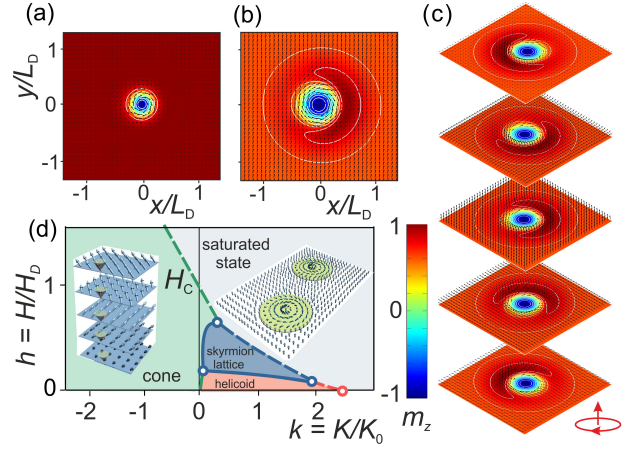


FIG. 1. Magnetic structures of chiral skyrmions at zero anisotropy (a-c): color plots of $m_z(x, y)$ (a) for an axisymmetric skyrmion in the saturated state ($h = 1.1$) and (b) for a non-axisymmetric skyrmion in the cone phase ($h = 0.6$); (c) a stack of magnetization planes $m_z(x, y)$ for different fixed values of z . In the generic phase diagram of noncentrosymmetric ferromagnets (d) common axisymmetric skyrmions (a) exist within the saturated phase and transform continuously into non-axisymmetric three-dimensional skyrmions (b) during the transition into the cone phase at critical line H_C .

non-axisymmetric skyrmions have been investigated in bulk¹² and confined chiral helimagnets¹³ but no experimental observations of these specific skyrmionic states have been reported to date.

In this Letter we report the first observations of non-axisymmetric skyrmions in the cone phase of a cubic helimagnet Cu_2OSeO_3 . We present real-space images of these clusters in Cu_2OSeO_3 acquired using transmission electron microscopy and provide a theoretical description of the experimental results.

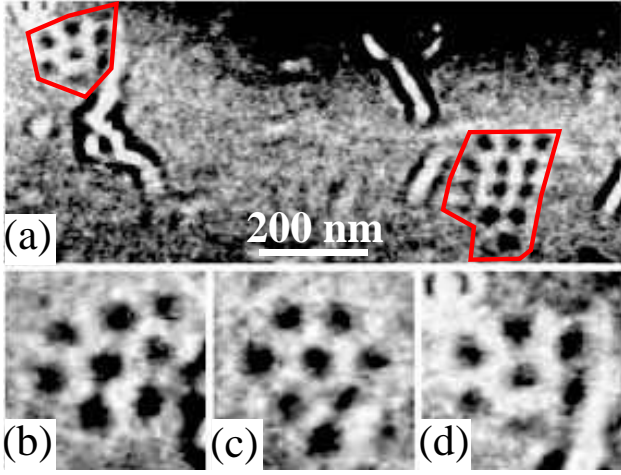


FIG. 2. Two skyrmion clusters (outlined in red) in the cone phase of Cu_2OSeO_3 at $T = 11$ K and $H = 116$ mT. (b)–(d) show changes in the shape of the left hand cluster with (c) taken 0.5 s and (d) taken 34.4 s after (b)

2. Chiral solitons and modulated phases are described mathematically by equations minimizing the energy functional of a chiral ferromagnet^{1,7}

$$w = A(\text{grad } \mathbf{M})^2 + K(\mathbf{M} \cdot \mathbf{n})^2 - \mu_0 \mathbf{M} \cdot \mathbf{H} + w_D, \quad (1)$$

where $\mathbf{M} = M(\sin \theta \cos \psi; \sin \theta \sin \psi; \cos \theta)$, A is the exchange stiffness constant, K is the uniaxial anisotropy constant, \mathbf{n} is the unity vector along uniaxial anisotropy axis, and \mathbf{H} is the applied magnetic field. The DM energy functionals w_D are composed of Lifshitz invariants $\mathcal{L}_{i,j}^{(k)} = M_i \partial M_j / \partial x_k - M_j \partial M_i / \partial x_k$ ^{1,3}. Skyrmions in the cone phase have the antiparallel magnetization on the skyrmion axis ($\theta_{\rho=0} = \pi$) and approach the solutions for the cone phase (θ_c, ψ_c)¹¹ at large distances from the axis⁷:

$$\theta_\infty = \theta_c = \arccos(H/H_C), \quad \psi_\infty = \psi_c = 2\pi z/L_D, \quad (2)$$

where $H_C = H_D(1 - K/K_0)$, $H_D = D^2 M / (2A)$, $L_D = 4\pi A / |D|$, $K_0 = D^2 / (4A)$ ¹¹. For an important case of non-centrosymmetric cubic ferromagnets (with space group $P2_13$), DM energy functional is reduced to the isotropic form: $w_D = D(\mathcal{L}_{yx}^{(z)} + \mathcal{L}_{xz}^{(y)} + \mathcal{L}_{zy}^{(x)}) = D \mathbf{M} \cdot \text{rot} \mathbf{M}^2$. The calculated phase diagram for this case is representative for a whole class of noncentrosymmetric ferromagnets (Fig. 1 (d))¹¹. In this phase diagram, the common axisymmetric skyrmions exist as ensembles of weakly repulsive strings within the magnetically saturated phase and non-axisymmetric skyrmions inhabit the cone phase (Fig. 1 (d)). During the phase transition from the saturated into the cone phase through the critical line H_C (Fig. 1 d) axisymmetric skyrmions continuously transform into non-axisymmetric skyrmions. In this paper we produce individual non-axisymmetric skyrmions and their clusters by the decomposition of the skyrmion lattices during the first-order transition into the cone phase.

3. Copper Oxy-Selenite (Cu_2OSeO_3) is a cubic helimagnet with the characteristic helical period $L_D = 63$ nm¹⁴. To acquire images of skyrmions, a single crystal of Cu_2OSeO_3 was thinned to electron transparency (about 70 nm) by the conventional process of mechanical grinding and argon-ion polishing on the (110) face. Lorentz transmission electron microscopy (LTEM) was conducted using an FEI Tecnai F20 electron microscope and the sample cooled *in-situ* using a liquid-helium cooled holder with a base temperature of 10 K. In the images produced using this technique, skyrmions appear as black or white circles and the cone phase does not produce any contrast variation. The results of our observations are presented in Figs. 2, 3, videos, and Figs. S1-SX collected in Supplement¹⁸.

Surface chiral twists arising in nanolayers of cubic helimagnets substantially influence the stability limits of the modulated phases⁶. As a result, skyrmion lattices exist in a broad range of the film thickness and applied magnetic fields and are separated from other modulated phases by the first-order transition lines (Fig. 3 d)^{15–17}. Recent experimental findings show that the first order transitions between the skyrmion lattice and cone phases in FeGe and MnSi nanolayers are accompanied by the formation and complex evolution of multidomain pattern consisting of domains with the competing phases^{15–17}. In our experiments, detailed investigations of the magnetic-field-driven evolution of such multidomain patterns have been resulted in the observation of skyrmion clusters (see Fig. 2 and attached Videos).

Fig. 2 shows frames from one of several videos we acquired showing two skyrmion clusters (outlined in red) coexisting with the cone phase in Cu_2OSeO_3 . The smaller cluster contained 7 skyrmions and the larger, 13. There does not appear to be a preferred number of skyrmions in a cluster and in other videos we observed a single skyrmion as well as clusters of 6, 18 and 21 skyrmions. In all of the videos we recorded, the skyrmions were in constant motion as shown in panels (b)–(d). Similar motion has been reported by Mochizuki *et al.*¹⁹ who attribute this to the heating of the specimen by the electron beam. We suggest instead that it is caused by specimen charging as coating the sample in a thin layer of carbon to improve its electrical conductivity eliminated the rotation and slowed the movement of the skyrmions.

Fig 3 was taken under the same conditions from a different region of the sample. It shows the skyrmion lattice phase coexisting with the cone phase and a cluster of 30 skyrmions moving towards and merging with the skyrmion lattice over 21 s. The boundaries of the cluster and the edge of the skyrmion lattice phase are delineated by red lines and by comparing panels (b) and (c), it can be seen that the phase boundary advances after merging is complete and that the skyrmions in the cluster have spread evenly across the boundary. Merging with the skyrmion lattice shows that these clusters occur at the phase boundary between the skyrmion lat-

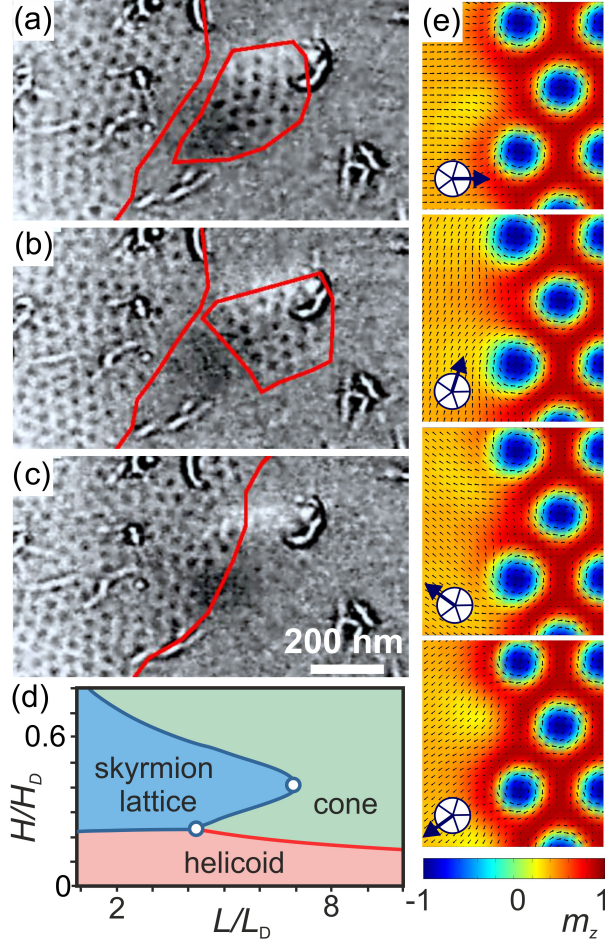


FIG. 3. LTEM images in a Cu_2OSeO_3 nanolayer of thickness $L = 70$ nm at $H = 116$ mT and $T = 12$ K (a-c) indicate the coexisting domains of the skyrmion lattice and cone phases during the first-order transition between these phases. (b) was taken 1.6 s after (a) and (c) 21.2 s after (a). The boundaries of the cluster and the skyrmion lattice are outlined in red. A sketch of the phase diagram of cubic helimagnet nanolayers includes areas with the helicoid, cone, and skyrmion lattices phases separated with the first-order transition lines (solid lines) (adopted from Ref.¹⁷) (d). The calculated domain wall between the coexisting skyrmion lattice and cone phases at the first-order transition line (e).

tice and cone phases. Areas with the cone and skyrmion lattice phases are separated by domain walls. The calculated contour plots of a such domain wall is presented in Fig. 3 (e). The frontal parts of skyrmion cores in the wall have a similar structure as those in non-axisymmetric skyrmions and play a role of nuclei for individual non-axisymmetric skyrmions. The attractive interaction between such skyrmions¹² explains the formation of skyrmion clusters observed in our experiments.

4. A non-axisymmetric skyrmion can be thought as a result of a continuous transformation of axisymmetric skyrmion during the phase transition from the saturated

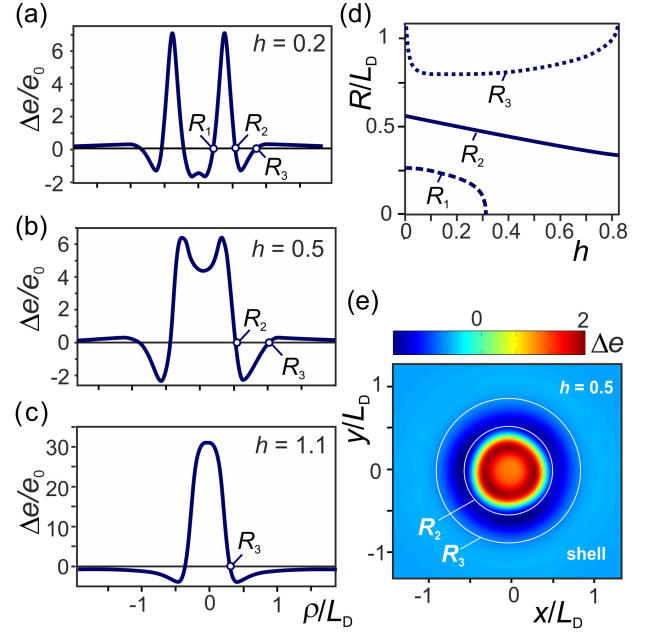


FIG. 4. (color online). Radial energy density profiles $\Delta e(\rho)$ (3) at zero anisotropy and different values of the applied field plotted in units $e_0 = 4\pi D$. (a-c). Characteristic radii R_i are plotted as functions of the applied field in fig.(d). In the cone phase (a,b) the skyrmion core is enclosed by positive "shells" ($\rho > R_3$) providing the attractive inter-skyrmion potential. Negative asymptotics of the radial energy density for axisymmetric skyrmions ($h > 1$) impose the repulsive skyrmion-skyrmion interaction (c). The contour plot $e(x, y)$ calculated for $h = 0.5$ (fig. (e)) shows the central part with large positive energy ($\rho < R_2$), the negative energy "belt" ($R_2 < \rho < R_3$), and the extended "shell" ($\rho > R_3$).

into the cone phase (Fig. 1 d). The equilibrium structure of a non-axisymmetric skyrmion is reached by the compatibility of the axisymmetric skyrmion core with the transversely modulated cone phase (Fig. 1 a-c)^{12,13}. The skyrmion core is separated from the host phase by a broad asymmetric "shell".

The numerical calculations presented in Fig. 4 elucidate the main features of non-axisymmetric skyrmions and their bound states. The calculated radial skyrmion energy densities

$$e(\rho) = (2\pi L_D)^{-1} \int_0^{L_D} dz \int_0^{2\pi} d\varphi w_s(\theta, \psi) \quad (3)$$

are plotted as functions $\Delta e(\rho) = (e(\rho) - e_{\text{cone}})$ for different values of the applied field (Fig. 4) where $w_s(\theta, \psi)$ is the energy density (1) for an isolated non-axisymmetric skyrmion and e_{cone} is energy density (3) calculated for the cone phase (2).

The characteristic lengths R_1 , R_2 , R_3 indicate several distinct regions in the radial energy density profiles $\Delta e(\rho)$ (Fig. 4 (c) -(e)). The functions $R_i(h)$ are plotted in Fig. 4 (d). For axisymmetric skyrmions (Fig. 4 (c)) the energy densities $\Delta e(\rho)$ consist of

the positive energy “bag” located in the skyrmion center ($\rho < R_2$) and encompassed by extended areas with negative energy density, where the DM coupling dominates⁴. Negative asymptotics of the radial energy densities ($\Delta e(\rho) < 0$ for $\rho \gg 1$) predetermines the *repulsive* inter-soliton potential for axisymmetric skyrmions⁴. For non-axisymmetric skyrmions (Figs. 4 (a), (b)) the energy densities $\Delta e(\rho)$ are positive at large distances from the skyrmion center ($\rho > R_3$). These areas correspond to “shells” separating the skyrmion core from the cone phase. The positive energy density of the “shell” leads to the “attractive” interactions between non-axisymmetric skyrmion¹². In other words, the phenomenon of the skyrmion-skyrmion attractive interaction in the cone phase is explained by the excessive energy density of the asymmetric shell (compared to those in the skyrmion core and the cone phase)¹². Importantly, the equilibrium distribution of the magnetization in the “shell” determines the material parameters of the cluster: the bound energy and the distance between the constituent skyrmions.

Another type of attractive chiral skyrmions have been earlier investigated theoretically in the *precursor* region of cubic helimagnets²⁰. It was shown that due to the “softening” of the magnetization near the ordering temperature, the skyrmion-skyrmion coupling acquires an oscillatory character and promotes the formation of skyrmion clusters in this region²⁰. The solutions for two-dimensional (*baby*) skyrmions with the oscillatory inter-particle potential have been also derived within the canonic Skyrme model²¹. In magnetism the Skyrme model is applied to describe a group of magnetic compounds with competing exchange interactions. *Ab-initio* calculations of attractive two-dimensional localized states in these magnetic systems have been carried out by Rozsa et al.²³. It was also found that the solutions for attractive baby-skyrmions exist in modified Faddeev-Skyrme models with a Lennard-Jones type potential term describing a short-range repulsion and a long-range attraction²².

The oscillatory vortex-vortex interaction attributed to type-II superconductors with small values of the Ginzburg-Landau parameter²⁴ leads to the first-order transition from the superconducting state into the Abrikosov vortex phase accompanied with the multidomain states of the competing phases²⁵. Vortex clusters stabilized by the oscillatory inter-vortex coupling have been observed in MnB_2 ²⁶ and Sr_2RuO_4 ²⁷.

The attractive skyrmions in the cone phase of noncentrosymmetric ferromagnets represent an alternative to solitons with the oscillatory inter-particle potential investigated in^{20,21,23–27}.

In conclusion, the first direct observations of attractive non-axisymmetric skyrmions and their clusters are reported in the cone phase of noncentrosymmetric ferromagnet. We obtained real-space images of skyrmion clusters and multidomain patterns during the phase transition between the cone and skyrmion lattice phases in a thin layer of cubic helimagnet Cu_2OSeO_3 by using

Lorentz transmission electron microscopy. The method for the formation of skyrmion clusters introduced in this paper is based on the magnetic-field-induced fragmentation of skyrmion lattice domains during the first-order transition into the cone phase. This method can be used to produce and investigate skyrmion clusters in the cone phases of other noncentrosymmetric ferromagnets.

The authors are grateful to K. Inoue, D. McGrouther, T. Monchesky, and Y. Togawa for useful discussions. This work was funded by the Royal Society (United Kingdom) and by JSPS Core-to-Core Program, A. Advanced Research Networks (Japan). M.C.H. and G.B. acknowledge financial support from EPSRC, United Kingdom.

I. SUPPLEMENTARY INFORMATION

A. Experimental Methods

Cu_2OSeO_3 single crystal samples of size 3 mm were grown by the vapour transport technique as described in ref. 14. These showed clear facets and the sample was thinned for electron microscopy by mechanically polishing on a (110) face until it was 20 μm thick. It was then further thinned by argon ion beam irradiation using a Gatan Precision Ion Polishing System (PIPS) initially operated at 4 kV with the ion guns set at 7° to the sample plane. Once the sample thickness approached the wavelength of light, rainbow colours could be observed using an optical microscope and, at this point, the voltage was reduced to 2 kV and the gun angle to 5° and thinning continued until a hole of size 15 μm appeared.

Transmission electron micrographs were taken from an area of sample approximately 70 nm thick surrounding this hole with an FEI Tecnai F20 transmission electron microscope (TEM) equipped with a field-emission gun using an acceleration voltage of 200 kV. In normal operation, the objective lens of the microscope applies a 2 T field to the specimen which would force it into the saturated state. Images were instead acquired in low-magnification mode in which the image is formed using the diffraction lens and the objective lens was weakly excited to apply a small magnetic field normal to the plane of the specimen.

The sample was cooled using a Gatan liquid-helium cooled IKHCHDT3010-special tilt-rotate holder which has a base temperature of 10 K. The images were energy-filtered so that only electrons which had lost between 0 and 10 eV on passing through the specimen contributed to the image and recorded on a video rate CCD camera at 25 frames per second. An aperture was used to ensure that only the 000-beam and the low-angle scattering from the skyrmions contributed to the image.

The defocus and magnification were calibrated by acquiring images with the same lens settings from Agar Scientific’s S106 calibration specimen, which consists of lines spaced by 463 nm ruled on an amorphous film. The defocus was found by taking digital Fourier transforms

of these images and measuring the radii of the dark rings that result from the contrast transfer function using the method described in ref. 28.

Magnetic phenomena can be visualised using electron microscopy as the Lorentz force from the magnetic flux in the specimen deflects the electron beam as it passes through and the magnetic structure can be seen in out-of-focus images on a scale of nanometres. Magnetic helices appear as black and white stripes and skyrmions appear as black or white dots. Neither the cone or saturated phases produce any contrast in a defocused image.

B. Videos of Skyrmion Clusters

Video 1 corresponds to Fig. 2 of the main paper and shows two skyrmion clusters in the cone phase of

Cu_2OSeO_3 at 11 K in an applied field of 110 m. As with all the videos, the spacing between the skyrmions is 60 nm and the video is shown in real time. All the videos were taken under very similar conditions from different regions of the sample.

Video 2 shows two more skyrmion clusters recorded at 12 K and 116 mT.

Video 3 corresponds to Fig. 3 of the main paper and shows a skyrmion cluster joining the skyrmion lattice at 12 K and 116 mT.

* j.c.loudon@gmail.com

† A.Leonov@ifw-dresden.de

¹ I. E. Dzyaloshinskii, Sov. Phys. JETP **19**, 960 (1964), **20**, 665 (1964).

² P. Bak and M. H. Jensen, J.Phys. C **13**, L881 (1980).

³ A. N. Bogdanov and D. A. Yablonskii, Sov. Phys. JETP **68**, 101 (1989).

⁴ A. Bogdanov and A. Hubert, J. Magn. Magn. Mater. **138**, 255 (1994), **195**, 182 (1999); A. Bogdanov, JETP Lett. **62**, 247 (1995).

⁵ N. Romming et al. Science **341**, 636 (2013).

⁶ M. N. Wilson et al., Phys. Rev. B **88**, 214420 (2013); S. A. Meynell et al., Phys. Rev. B **90**, 014406 (2014).

⁷ A. O. Leonov et al., New J. of Phys. **18**, 065003 (2016).

⁸ U. K. Rößler, A. N. Bogdanov, C. Pfleiderer, Nature (London), **442**, 797 (2006).

⁹ C. Melcher, Proc. R. Soc. A **470**, 20140394 (2015).

¹⁰ N. S. Kiselev et al., J. Phys. D: Appl. Phys. **44**, 392001 (2011); A. Fert, V. Cros, and J. Sampaio, Nat. Nanotechnol. **8**, 152 (2013).

¹¹ A. B. Butenko et al., Phys. Rev. B **82**, 052403 (2010); M. N. Wilson et al., Phys. Rev. B **89**, 094411 (2014).

¹² A. O. Leonov et al., J. Phys.: Condens. Matter. **28**, 35LT01

(2016).

¹³ A. O. Leonov, J. C. Loudon, A. N. Bogdanov, Appl. Phys. Lett. **109**, 172404 (2016).

¹⁴ S. Seki et al., Science **336**, 198 (2012).

¹⁵ X. Z. Yu et al., Nature Comm. **3**, 988 (2012).

¹⁶ X. Z. Yu et al. Phys. Rev. B **91**, 054411 (2015).

¹⁷ A. O. Leonov et al. Phys. Rev. Lett. **117**, 087202 (2016).

¹⁸ Supplement.

¹⁹ M. Mochizuki et al. Nature Mat. **13**, 241 (2014).

²⁰ H. Wilhelm et al. Phys. Rev. Lett. **107**, 127203 (2011); J. Phys.: Condens. Matter **24**, 127203 (2012).

²¹ A. O. Leonov and M. Mostovoy, Nat. Commun. **6**, 8275 (2015).

²² P. Salmi and P. Sutcliffe, J. Phys. A: Math. Theor. **48**, 035401 (2015).

²³ L. Rozsa et al. Phys. Rev. Lett. **117**, 157205 (2016).

²⁴ A. Hubert, Phys. Lett. **36A**, 359 (1971).

²⁵ U. Essmann, Physica, **55**, 83 (1971).

²⁶ V. Moshchalkov et al. Phys. Rev. Lett. **91**, 117001 (2009); J. Gutierrez et al. Phys. Rev. B **85**, 094511 (2012).

²⁷ P. J. Curran et al. Phys. Rev. B **84**, 104507 (2011).

²⁸ D. B. Williams and C. B. Carter, *Transmission Electron Microscopy* (Springer, New York, 1996) Chap. 28.